Eur. Phys. J. D (2017) 71: 218
DOI: 10.1140/epjd/e2017-70763-0

THE EUROPEAN PHYSICAL JOURNAL D

Regular Article

Coherent electron emission from O_2 in collisions with fast electrons

Madhusree Roy Chowdhury[1], Carlos R. Stia[2], Carmen A. Tachino[2], Omar A. Fojón[2], Roberto D. Rivarola[2], and Lokesh C. Tribedi[1,a]

[1] Tata Institute of Fundamental Research, Homi Bhabha Road, 400005 Mumbai, India
[2] Instituto de Física Rosario (CONICET-UNR), 2000 Rosario, Argentina

Received 6 December 2016 / Received in final form 21 February 2017
Published online 29 August 2017 –

Abstract. Absolute double differential cross sections (DDCS) of secondary electrons emitted in ionization of O_2 by fast electrons have been measured for different emission angles. Theoretical calculations of atomic DDCS were obtained using the first Born approximation with an asymptotic charge of $Z_T = 1$. The measured molecular DDCS were divided by twice the theoretical atomic DDCS to detect the presence of interference effects which was the aim of the experiment. The experimental to theoretical DDCS ratios showed clear signature of first order interference oscillation for all emission angles. The ratios were fitted by a first order Cohen-Fano type model. The variation of the oscillation amplitudes as a function of the electron emission angle showed a parabolic behaviour which goes through a minimum at 90°. The single differential and total ionization cross sections have also been deduced, besides the KLL Auger cross sections. In order to make a comparative study, we have discussed these results along with our recent experimental data obtained for N_2 molecule.

1 Introduction

Cross section measurements of electron impact ionization of different atoms and molecules have been a subject of study over decades. Several theoretical and experimental works have been executed to measure the total ionization cross section (TCS) or single differential cross section (SDCS) for different target species. The cross sections, differential over electron emission energy and angle, provide more detailed picture of the collision mechanisms. The DDCS measurements of O_2 and N_2 induced by intermediate energy electrons have been performed previously [1].

Apart from differential cross section measurements, another interesting feature of diatomic molecules is its resemblance with Young's double slit for electron waves where the two nuclei act as the two slits, as predicted by Cohen and Fano in 1966 [2]. Electrons are emitted coherently from the two centers of the molecule giving rise to interference oscillations. Several works towards the interference effect have been carried out in case of the simplest diatomic molecule, H_2 in collisions with fast electrons, heavy ions or photons [3–6]. Extending the work further from H_2 to more complex diatomic molecules, such as N_2 and O_2, oscillation has been observed in individual orbitals when impacted with photons [7]. The oscillations observed in individual orbitals were phase shifted from each other. For heavy ion impact, there lies some controversy about the evidence of oscillation both for N_2 and O_2 [8–10]. However, for proton impact on N_2, it has been theoretically shown that interference signatures appear in double differential cross sections (DDCS) for the two innermost molecular orbitals, being them in phase opposition [11]. Recently, the interference related experiments have also been performed for heteronuclear molecules [12,13].

In this work, we aim to investigate the presence of interference effect for the multi-electronic target O_2 upon impact with fast electrons of energy 7 keV. Recently interference oscillation have been observed in triple [14] and double [15] differential cross section measurements of N_2 by intermediate and high energy electrons respectively. To our knowledge, no such observation has been reported for electron impact ionization of O_2 (except a very recent work, indicated below). In case of fast electron beam as projectile, the Coulomb perturbation strength is quite small compared to fast heavy ions (e.g. C or O ions) of similar velocity for which simultaneous multiple ionization of different orbitals are quite strong. In this respect the electrons can be considered as a "gentle" projectile resulting in negligible multiple ionization. In this work we will mainly talk about the interference oscillations observed for oxygen molecule from the DDCS ratios. Though detailed discussions about interference oscillations for N_2 have been reported in reference [15], to make a comparative study for the two molecules we have added some of our recent and detailed data of N_2 which are not shown in [15] along with the data for molecular oxygen. As explained below,

[a] e-mail: lokesh@tifr.res.in

the ratio of DDCS for O_2-to-2O (i.e. twice the atomic DDCS) was used to derive the interference oscillation.

In the absence of experimental atomic cross sections, the DDCS for atomic oxygen were obtained from a theoretical formalism, where the multielectronic system was reduced to a single effective electron problem. In a similar manner, the DDCS for atomic N were also obtained. Since the main goal of this work is to explore the interference oscillation through the study of DDCS ratios, we do not make any attempt to predict the molecular DDCS, as proper molecular calculations are at present in progress. Detailed discussion on the theoretical formalisms concerning the coherent electron emission from different target molecules are discussed in reference [16]. Further details of theoretical work in connection with the N_2 ionization is given in our recent work [15]. Atomic units are used unless otherwise stated.

2 Experimental details

The projectile electrons of energy 7 keV was obtained from a commercially available electron gun. The beam was focussed and collimated using Einzel lens, electrostatic deflectors and several apertures of different diameters. Magnetic coils were also used for better alignment. A stable beam of about 900 nA current was used throughout the experiment with minor fluctuations in the presence and absence of gas.

The experiment was performed in high vacuum condition at a base pressure of 5×10^{-8} mbar. The chamber was flooded with the target gases (O_2, N_2) at an absolute pressure of 0.15 mTorr which was monitored with a capacitance manometer. The electrons ejected after collision with the projectile beam were energy analyzed with the help of a hemispherical analyzer and further detected by a channel electron multiplier (CEM). The entire spectrometer was kept on a motorized turntable. The front of the CEM was biased at positive potential of 100 V, since the detection efficiency of CEM remains fairly constant (∼85%) within an electron energy range of about 100–700 eV. The entrance and exit slits were biased with a pre-acceleration voltage of 6 V which enhanced the collection of the low energy electrons. The Earth's magnetic field was reduced to about 10 mG near the interaction region. The low magnetic field was achieved with two sets of μ-metal sheets lined on the inner wall of the scattering chamber. The incident beam was collected on a Faraday Cup for beam normalization purpose. The Faraday Cup was sufficiently long in order to prohibit the back scattered electrons from reaching the interaction region. The projectile beam transmission was obtained by comparing the current from two positions of the analyzer, i.e. aligned along 0° and then by moving it away from the beam path. When the analyzer is placed in-line with the beam direction, the projectile beam had to pass through several (i.e. five) apertures on the spectrometer, apart from the ones used for beam collimation, before falling on the Faraday cup. In the present experiment, the beam transmission was ∼85%.

The secondary electrons were collected for different emission angles between 15° and 145°. At each angle, electrons emitted with energy from 1–600 eV and 1–550 eV were detected for O_2 and N_2 respectively. The energy resolution of the analyser was ∼6% where the contribution from acceptance angle is about 1%. The sources of uncertainties in the DDCS measurement were from the statistical fluctuation (2%–10%), gas pressure fluctuation (6%–7%), efficiency (10%), resolution (5%–10%) and solid-angle-path-length integral (10%–12%). Overall error was estimated to be around 20%.

3 Theory

In the present study the interest is focused in the case of electrons as projectiles. A detailed analysis of the calculation of DDCS for electron emission from diatomic molecules by impact of protons and electrons was given in a recent review [16] and references therein.

As the possible existence of interference patterns is explored here from the ratio between experimental molecular DDCS and atomic DDCS corresponding to each one of the atomic compounds of the molecule, we pay particular attention to the determination of the latter ones.

In order to calculate the atomic cross sections, within the framework of an independent electron model, it is assumed that only one target electron (the *active* one) is ionized in the final channel of the reaction, whereas the remaining *passive* electrons are considered as frozen in their initial orbitals during the reaction. In this context, DDCS were determined within a first-order Born approximation (B1), where the projectile dynamics is described through a plane-wave, in both the initial and final channels. In the entry channel, a Roothaan-Hartree-Fock representation of the different atomic orbitals was employed [17] and in the exit one, a Coulomb residual continuum function with an effective charge Z_T of unity was taken. This charge may be interpreted as the asymptotic one felt by the ionized electron due to its interaction with the residual target.

4 Results and discussions

4.1 Energy distribution of DDCS spectrum

Figure 1 displays the energy distributions of the secondary electrons ejected from O_2 molecules. The solid line corresponds to twice the atomic oxygen calculations. They are seen to be close to data points for the extreme forward and backward angles, whereas the difference is largest in case of angles near 90°. The sharp peak around 480 eV for all emission angles correspond to the K-LL Auger electron emission which is shown in the insets in Figure 1.

The energy distribution of the secondary electrons emitted in collision of 7 keV electrons with N_2 target is shown in Figure 2 for different emission angles. Theoretical calculations for twice the atomic nitrogen are also shown. The K-LL Auger electrons for nitrogen are emitted around

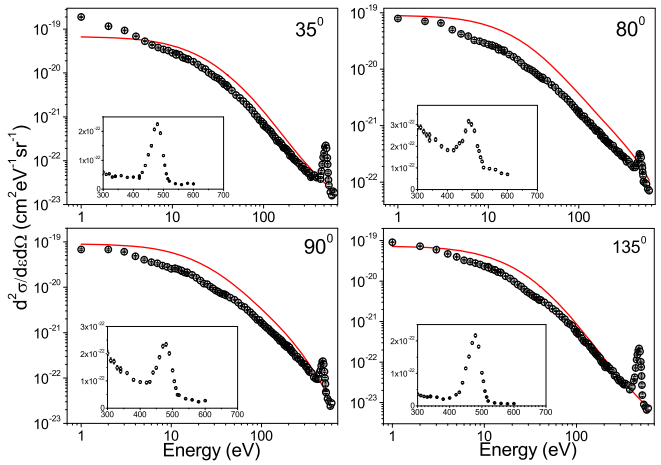

Fig. 1. The measured absolute DDCS of O_2 for different emission angles. The red solid line corresponds to twice atomic O calculation using $Z_T = 1$. The Auger peak for each angle is shown separately in the insets.

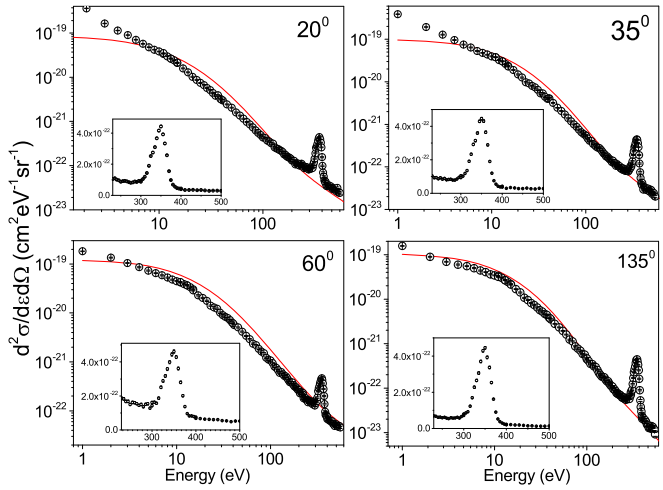

Fig. 2. Absolute electron DDCS of N_2 at different forward and backward emission angles; Auger peaks are shown in the insets. The theoretical cross sections for twice atomic nitrogen (red solid line) are calculated using $Z_T = 1$.

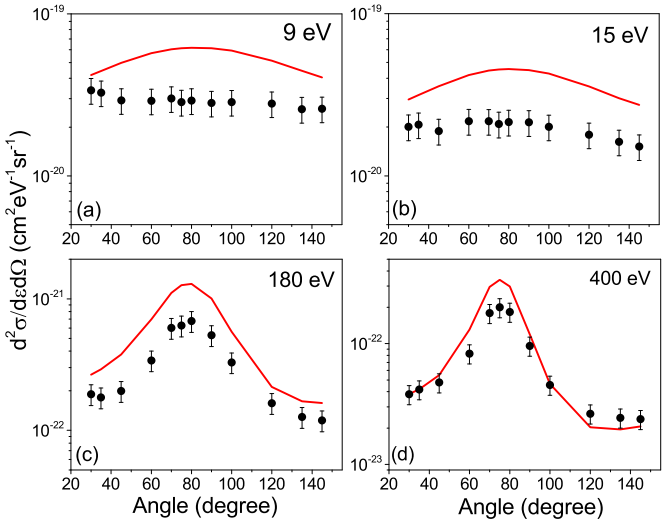

Fig. 3. DDCS at fixed electron emission energies for O_2. The red solid line corresponds to the theoretical calculations for 2O.

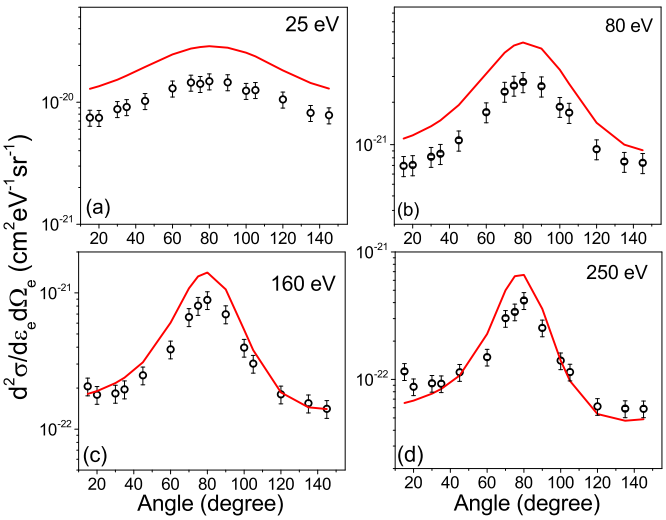

Fig. 4. DDCS for N_2 at fixed electron emission energies along with theoretical calculations for 2N (solid lines).

355 eV, which is seen by the sharp peak in the DDCS spectrum (insets in Fig. 2). In case of extreme forward angles (20° and 35°), the cross section is seen to have a sharp rise for lowest emission energies (≤5 eV) unlike that observed from the calculations. Although the origin of such unusual rise is not understood, but a systematic error due to unsubtracted slit-scattering background can not be ruled out completely.

4.2 Angular distribution of DDCS spectrum

The angular distribution of the secondary electrons emitted from O_2 and N_2 are displayed in Figures 3 and 4 respectively. Tables 1 and 2 display some of the selected DDCS values, for a ready reference. The solid lines in Figure 3 correspond to twice the theoretical calculations of atomic oxygen. The atomic cross sections are seen to be larger than the measured DDCS for molecular target with the discrepancy being largest for low emission energies. The distribution is seen to be almost flat for low emission energies which is governed by soft collision mechanisms. Here the electrons are emitted with large impact parameter. With increase in emission energy, a peaking is observed around 80° which is explained in terms of the binary nature of the collision. Similar distributions for N_2 are also observed (shown in Fig. 4). The red curves represent the theoretical calculations for 2N. Though overall qualitative matching is observed, theory underestimates the data for all cases. A minor signature of forward-backward asymmetry is observed for O_2 for higher emission energies.

Table 1. Measured DDCS for N_2 in units of Mb eV^{-1} sr^{-1} for different emission angles.

Energy (eV)	15°	20°	35°	45°	60°	70°	75°	80°	90°	100°	105°	120°	135°	145°
3	–	0.163	0.128	0.113	0.105	0.102	0.0983	0.092	0.0778	0.0568	0.0818	0.0644	0.0693	0.0724
5	–	0.089	0.075	0.0713	0.073	0.0725	0.0719	0.0684	0.0655	0.051	0.0647	0.0512	0.0554	0.0554
10	0.045	0.038	0.039	0.0394	0.0446	0.047	0.0458	0.0456	0.0444	0.0403	0.043	0.0346	0.0342	0.0334
21	0.0106	0.0102	0.0126	0.0135	0.0176	0.018	0.0184	0.0188	0.0186	0.0161	0.0169	0.013	0.0107	0.0105
41	3.1E-3	2.9E-3	4.1E-3	4.5E-3	5.6E-3	6.5E-3	7.1E-3	7.8E-3	7.6E-3	6.4E-3	6.7E-3	4.4E-3	3.5E-3	3.1E-3
60	1.4E-3	1.4E-3	1.7E-3	1.9E-3	2.9E-3	3.6E-3	4.2E-3	4.1E-3	3.9E-3	3.1E-3	2.9E-3	1.9E-3	1.6E-3	1.4E-3
100	4.6E-4	4.3E-4	5.5E-4	6.5E-4	1.1E-3	1.5E-3	1.7E-3	1.8E-3	1.7E-3	1.2E-3	1.02E-3	5.7E-4	4.5E-4	4.4E-4
140	2.8E-4	2.4E-4	2.8E-4	3.3E-4	5.2E-4	8.0E-4	1.1E-3	1.1E-3	9.4E-4	5.2E-4	4.3E-4	2.6E-4	2.01E-4	1.9E-4
180	1.7E-4	1.5E-4	1.5E-4	1.9E-4	3.1E-4	5.7E-4	7.4E-4	7.6E-4	5.6E-4	2.9E-4	2.4E-4	1.3E-4	1.2E-4	1.1E-4
220	1.3E-4	1.1E-4	1.1E-4	1.5E-4	2.3E-4	3.9E-4	5.2E-4	5.4E-4	4.0E-4	1.7E-4	1.6E-4	8.6E-5	7.3E-5	7.4E-5
250	1.1E-4	8.8E-5	9.3E-5	1.1E-4	1.5E-4	3.0E-4	3.4E-4	4.2E-4	2.5E-4	1.4E-4	1.1E-4	6.1E-5	5.9E-5	5.9E-5

Table 2. Measured DDCS for O_2 in units of Mb eV^{-1} sr^{-1} for different emission angles.

Energy (eV)	30°	35°	45°	60°	70°	75°	80°	90°	100°	120°	135°	145°
3	0.0993	0.0933	0.071	0.0672	0.0655	0.0632	0.0654	0.0606	0.0542	0.0675	0.0601	0.0646
5	0.0586	0.0533	0.0445	0.0421	0.0419	0.0415	0.0424	0.0405	0.0401	0.0408	0.0398	0.0383
10	0.0303	0.0288	0.0265	0.0279	0.0282	0.0284	0.0273	0.0256	0.0278	0.0257	0.0232	0.0238
21	0.0146	0.013	0.0137	0.0151	0.0152	0.0148	0.0147	0.014	0.0142	0.0114	9.7E-3	8.6E-3
41	4.4E-3	4.7E-3	4.9E-3	6.5E-3	6.9E-3	6.6E-3	6.6E-3	6.6E-3	5.4E-3	4.1E-3	3.4E-3	3.03E-3
60	2.2E-3	2.3E-3	2.7E-3	3.3E-3	4.1E-3	3.8E-3	4.0E-3	3.9E-3	3.4E-3	2.4E-3	1.8E-3	1.7E-3
100	6.4E-4	7.0E-4	8.6E-4	1.2E-3	1.5E-3	1.7E-3	1.8E-3	1.7E-3	1.3E-3	6.9E-4	5.8E-4	5.4E-4
140	2.8E-4	2.8E-4	3.7E-4	6.1E-4	9.5E-4	9.4E-4	9.7E-4	8.9E-4	5.8E-4	3.1E-4	2.4E-4	2.5E-4
180	1.8E-4	1.8E-4	1.9E-4	3.4E-4	6.0E-4	6.2E-4	6.8E-4	5.3E-4	3.3E-4	1.6E-4	1.3E-4	1.2E-4
220	1.1E-4	1.0E-4	1.3E-4	2.5E-4	4.1E-4	4.9E-4	4.8E-4	3.7E-4	2.0E-4	8.7E-5	7.2E-5	7.7E-5
260	7.3E-5	7.1E-5	8.8E-5	1.7E-4	3.4E-4	3.4E-4	3.6E-4	2.6E-4	1.2E-4	5.3E-5	4.6E-5	5.0E-5
300	6.2E-5	5.9E-5	6.9E-5	1.3E-4	2.8E-4	2.9E-4	2.9E-4	2.01E-4	7.8E-5	4.4E-5	3.6E-5	3.02E-5
340	4.9E-5	4.4E-5	4.8E-5	9.7E-5	2.3E-4	2.4E-4	2.5E-4	1.5E-4	5.5E-5	3.2E-5	2.8E-5	2.5E-5
400	3.8E-5	4.2E-5	4.8E-5	8.3E-5	1.8E-4	2.0E-4	1.8E-4	9.6E-5	4.5E-5	2.6E-5	2.4E-5	2.4E-5

In Figure 5 we have shown the angular distribution of the Auger electron peak for O_2 and N_2. The KLL Auger electrons are emitted when K-shell ionization of the target atom takes place. As already seen from Figures 1 and 2, the peaks for O_2 and N_2 are seen around 480 eV and 355 eV, respectively, as expected. We have obtained the area under the Auger peak for each case. For an atom one may expect an isotropic angular distribution of the KLL Auger electron. In case of the O_2 molecule we do see such an isotropic behaviour (Fig. 5a). However, in the case of the N_2 molecules although the general behaviour is almost isotropic within about 15%, there is a oscillatory structure in the distribution (shown by the blue solid line in Fig. 5b, which is a guide to eye). The origin of such behaviour in the case of N_2 is not obvious. For the N and O atoms, the fluorescence yields are negligible. The total K-shell ionization cross sections, thus, derived from the K-LL Auger yield, are found to be 0.095 Mb for O_2 and 0.163 Mb for N_2.

4.3 Experimental-to-theoretical DDCS ratio

From Figures 1 and 2, it is seen that the cross sections for both molecular and atomic targets fall by several orders of magnitude within the detected electron energy range. On the other hand, the variation due to interference effects contributing from the molecule is rather small and hence cannot be observed readily from the DDCS spectrum.

In a previous work [15], DDCS for impact of electron beams on N_2 targets have been approximated by,

$$\sigma_{mol} = 2\sigma_{at}(k)\left[1 + \frac{\sin\left[kc(\theta)d\right]}{kc(\theta)d}\right] \quad (1)$$

where σ_{at} is the atomic cross section corresponding to each individual molecular compound, and $\frac{\sin[kc(\theta)d]}{kc(\theta)d}$ is a Cohen-Fano type term originated from the coherent electron emission from the molecule. Here k is the electron momentum, d is the internuclear distance of the diatomic molecule, and $c(\theta)$ is an adjustable frequency parameter. This expression has been employed just as an extension of the one obtained in collisions between ion beams and H_2 targets [2,5,18–20].

Therefore, to reveal the contribution due to interference effects, it is necessary to omit the variation of the cross section over the emission energy by dividing the molecular DDCS by twice the corresponding atomic cross section (see Eq. (1)). Due to the absence of measured data for the atomic target, the DDCS for O_2 are divided by the theoretical atomic calculations. In Figure 6, the DDCS ratios of O_2 to twice the theoretical cross sections of atomic

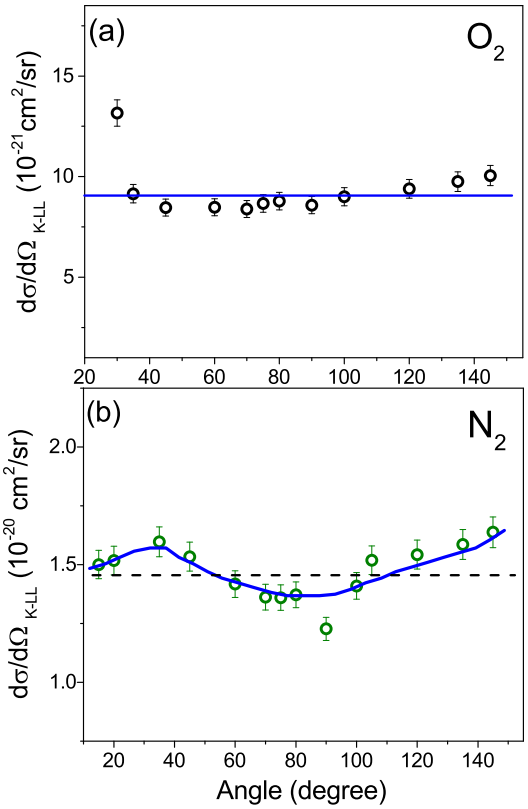

Fig. 5. Angular distribution of K-LL Auger electron emission for O_2 in (a) and N_2 in (b). Blue solid lines are a guide to eye.

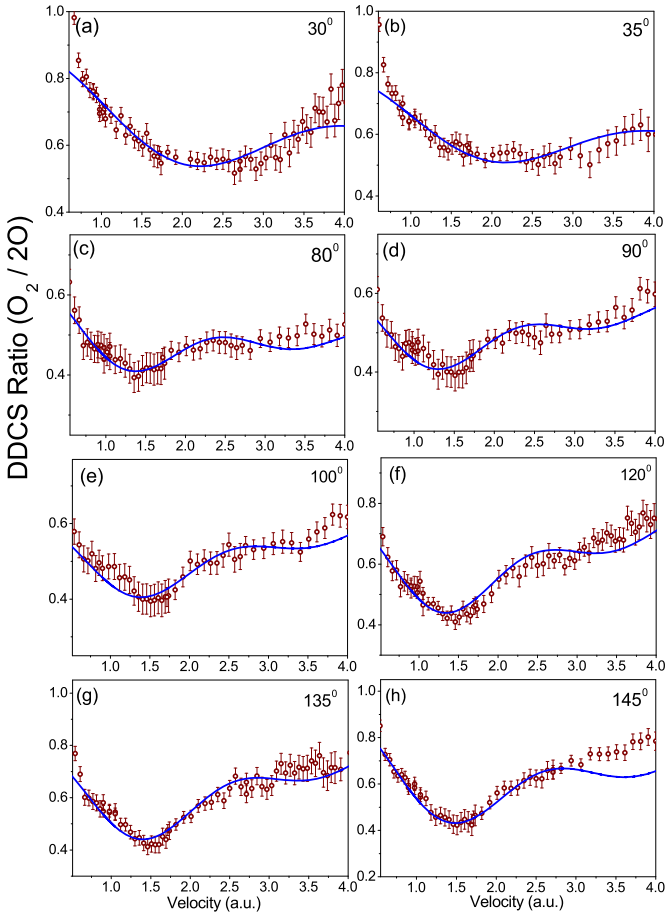

Fig. 6. Molecular to atomic cross section ratio ($\sigma_{O_2}/2\sigma_O$). Solid line represents the Cohen-Fano fitting given by equation (2).

oxygen are displayed for several forward and backward angles. The ratios reveal clear oscillatory structures for all the emission angles. In the case of 30° and 35°, half sinusoidal oscillatory structure is observed about a horizontal line. However, for other angles, full oscillation is observed. It may also be noticed that the oscillatory structure for the backward angles rides over a straight line of small positive slope. Also, a finer look into the ratio plots reveal that the oscillations are around 0.5–0.6, instead of the expected value of 1.0. These differences may be attributed to the fact, that the calculated atomic cross sections overestimate the data for all cases as can be readily seen from the energy distribution in Figure 1. To get a quantitative idea of the oscillatory structure with respect to electron velocity, the ratios have been fitted with the Cohen-Fano type model which is expressed as follows:

$$\frac{\sigma_{molecule}}{2\sigma_{atom}} = D + F(\theta)\frac{\sin\left[kc(\theta)d\right)]}{kc(\theta)d}. \qquad (2)$$

In this equation, $F(\theta)$ is the amplitude of the oscillation, k is the electron momentum, d is the internuclear distance (2.28 a.u. for O_2), and $c(\theta)$ is the variable frequency parameter. For most of the backward angles, to account for the minor increasing trend in the oscillation, we have added a linear term in equation (2) along with the Cohen-Fano term. The slope was found to be almost same for these angles. The fitting is seen to match quite well for all the angles.

Similar DDCS ratios for nitrogen molecule are shown in Figure 7. In the case of N_2, the data have been divided by the calculated cross sections of 2N. Half sinusoidal oscillations for all emission angles are also observed for N_2. The blue curve in each plot corresponds to the fitting given by equation (2). Here, a half sinusoidal oscillation is observed for all angles between 0.5 and 3.5 a.u. The fitted curve is seen to match well upto 3 a.u. for all angles except for 135°. By comparing Figures 6 and 7, it may be observed that for extreme forward angles (20°, 30°, 35°) the frequency of oscillation is almost same for O_2 and N_2. However, for extreme backward angles (e.g. 135°), the frequency for O_2 is much larger than that for N_2.

The variation of the oscillation amplitude as a function of the emission angle for both O_2 and N_2 is shown in Figure 8. The green open circles correspond to the amplitude variation for O_2 whereas the blue open triangles are that for N_2. For both the targets, the amplitude is seen to be higher for the extreme forward and backward angles with the minimum being observed around 90°. Additional experimental and theoretical investigations need to be taken up in order to understand this behaviour. Though qualitatively the variation of the amplitude with angle is seen to be the same for O_2 and N_2, but quantitatively

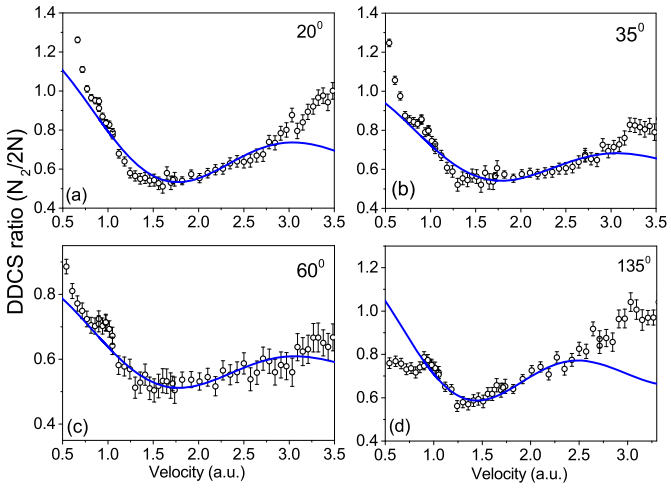

Fig. 7. DDCS ratio ($\sigma_{N_2}/2\sigma_N$). Blue solid line is the Cohen-Fano model fitting to the ratio points.

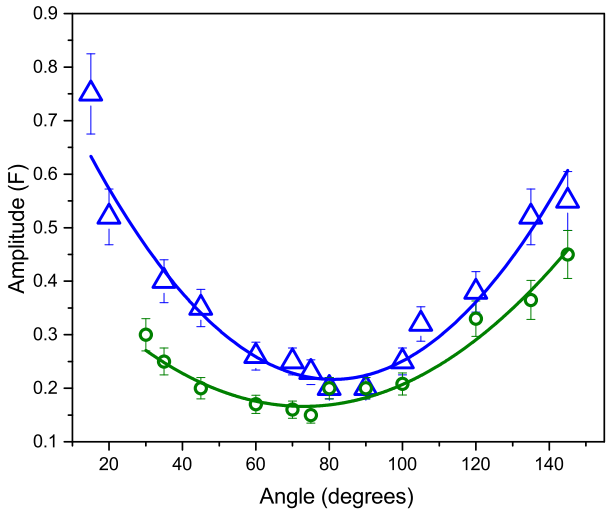

Fig. 8. Variation of oscillation amplitude as a function of the emission angle for O_2 and N_2. The blue open triangles and green open circles represent the data for N_2 and O_2 respectively. The fitted parabolic lines are shown as a guide to eye.

it is observed that the DDCS ratios for N_2 have higher amplitude of oscillation compared to that for O_2. In a very recent work [21] on e-impact ionization of O_2, the interference oscillation has been observed from the forward-backward angular asymmetry parameter which does not require any theoretical cross section.

4.4 Single differential cross section

The DDCS spectrum when integrated over the electron emission energy or emission angle gives the single differential cross section (SDCS). Integrating the DDCS spectrum over the emission energy gives the SDCS as a function of the emission angle:

$$\frac{d\sigma}{d\Omega_e} = \int \frac{d^2\sigma}{d\Omega_e d\epsilon_e} d\epsilon_e. \tag{3}$$

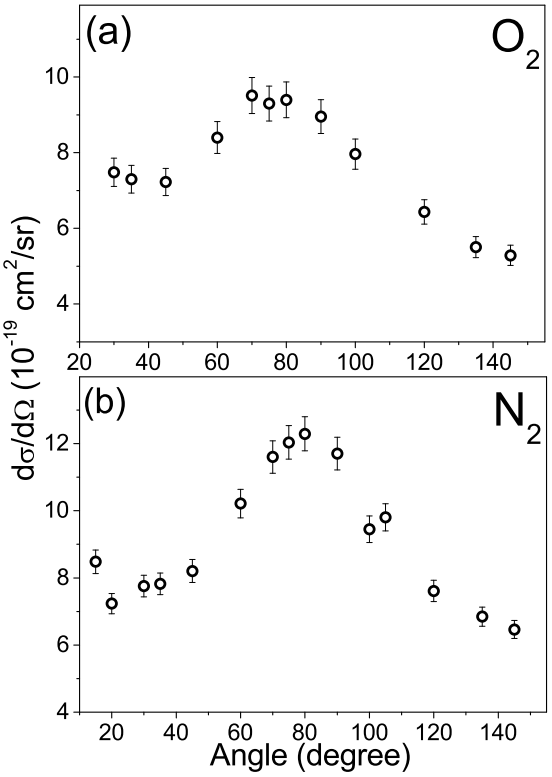

Fig. 9. Absolute electron SDCS for O_2 (a) and N_2 (b) as a function of the emission angle.

Similarly, integrating the DDCS spectrum over the emission angle provides the SDCS as a function of the emission energy:

$$\frac{d\sigma}{d\epsilon_e} = \int \frac{d^2\sigma}{d\epsilon_e d\Omega_e} d\Omega_e. \tag{4}$$

The variation of SDCS as a function of the emission angle is shown in Figures 9a and 9b for O_2 and N_2 respectively. The integration of the DDCS spectrum has been performed over an energy range of 5–340 eV for O_2 and 5–300 eV for N_2. From the figure, it is seen that the SDCS for the extreme forward angles remain almost constant. A peaking structure is observed around 80°. Minor signature of forward-backward asymmetry is seen in the SDCS spectrum for O_2 but no such angular asymmetry is observed for N_2.

Finally by integrating the DDCS spectrum over the energy and angular range we obtained the total cross section (TCS). The TCS was found to be 11.2 (±2.2) Mb for O_2 and 14.6 (±2.9) Mb for N_2.

5 Conclusion

The absolute DDCS of the secondary electrons emitted in ionization of O_2 by 7 keV electrons were measured for different forward and backward angles. The secondary electrons having energies between 1 and 600 eV have been detected. The evidence of interference oscillations for the diatomic molecules have been revealed in the DDCS-ratios. The oscillations were further fitted

by the Cohen-Fano model for interference in molecular double-slit. The frequency of the oscillation for O_2 was found to be higher than that for N_2 for extreme backward angles. Though in the case of fast heavy ion impact, interference oscillations for these molecules are not consensual, the present work reveals a clear signature of interference. This result, however, is in qualitative agreement with the observed oscillations in photoionization. In addition, the SDCS, the TCS and the KLL Auger electron cross sections have also been deduced.

The authors would like to thank Mr. W.A. Fernandes and Mr. Nilesh Mhatre for their help during the experiment.

Author contribution statement

L.C.T. had initiated the idea and developed the research; conducting experiment, analysis and interpretation were done jointly by M.R.C. and L.C.T.; C.R.S., C.A.T., O.A.F. and R.D.R. provided the theoretical calculations for the atomic targets; M.R.C. and L.C.T. wrote the paper with necessary inputs from R.D.R. and O.A.F.

References

1. C.B. Opal, W.K. Peterson, E.C. Beaty, J. Chem. Phys. **55**, 4100 (1971)
2. H.D. Cohen, U. Fano, Phys. Rev. **150**, 30 (1966)
3. N. Stolterfoht, B. Sulik, V. Hoffmann, B. Skogvall, J.Y. Chesnel, J. Rangama, F. Frémont, D. Hennecart, A. Cassimi, X. Husson, A.L. Landers, J.A. Tanis, M.E. Galassi, R.D. Rivarola, Phys. Rev. Lett. **87**, 023201 (2001)
4. D. Misra, U. Kadhane, Y.P. Singh, L.C. Tribedi, P.D. Fainstein, P. Richard, Phys. Rev. Lett. **92**, 153201 (2004)
5. D. Misra, A. Kelkar, U. Kadhane, A. Kumar, Y.P. Singh, L.C. Tribedi, P.D. Fainstein, Phys. Rev. A **75**, 052712 (2007)
6. S. Chatterjee, D. Misra, A.H. Kelkar, Lokesh C. Tribedi, C.R. Stia, O.A. Fojón, R.D. Rivarola, J. Phys. B **42**, 065201 (2009)
7. M. Ilchen, L. Glaser, F. Scholz, P. Walter, S. Deinert, A. Rothkirch, J. Seltmann, J. Viefhaus, P. Decleva, B. Langer, A. Knie, A. Ehresmann, M. Braune, G. Hartmann, A. Meissner, L. Tribedi, M. Al-Khaldi, O. Al-Dossary, U. Becker, Phys. Rev. Lett. **112**, 023001 (2014)
8. J.L. Baran, S. Das, F. Járai-Szábo, K. Póra, L. Nagy, J.A. Tanis, Phys. Rev. A **78**, 012710 (2008)
9. S. Nandi, A.N. Agnihotri, S. Kasthurirangan, A. Kumar, C.A. Tachino, R.D. Rivarola, F. Martín, L.C. Tribedi, Phys. Rev. A **85**, 062705 (2012)
10. S. Nandi, S. Biswas, C.A. Tachino, R.D. Rivarola, L.C. Tribedi, Eur. Phys. J. D **69**, 192 (2015)
11. C.A. Tachino, F. Martín, R.D. Rivarola, J. Phys. B **45**, 025201 (2012)
12. S.E. Canton, E. Plésiat, J.D. Bozek, B.S. Rude, P. Decleva, F. Martin, Proc. Natl. Acad. Sci. **108**, 7302 (2011)
13. R.K. Kushawaha, M. Patanen, R. Guillemin, L. Journel, C. Miron, M. Simon, M.N. Piancastelli, C. Stakes, P. Decleva, Proc. Natl. Acad. Sci **110**, 15201 (2013)
14. H. Chaluvadi, N.O. Zehra, M. Dogan, C. Ning, J. Colgan, D. Madison, J. Phys. B **48**, 155203 (2015)
15. M. Roy Chowdhury, C.R. Stia, C.A. Tachino, O.A. Fojón, R.D. Rivarola, L.C. Tribedi, Phys. Rev. A **94**, 053703 (2016)
16. M.F. Ciappina, O.A. Fojón, R.D. Rivarola, J. Phys. B **47**, 042001 (2014)
17. E. Clementi, C. Roetti, At. Data Nucl. Data Tables **14**, 177 (1974)
18. L. Nagy, L. Kocbach, K. Póra, J.P. Hansen, J. Phys. B **35**, L453 (2002)
19. N. Stolterfoht, B. Sulik, L. Gulyás, B. Skogvall, J.Y. Chesnel, F. Frémont, D. Hennecart, A. Cassimi, L. Adoui, S. Hossain, J.A. Tanis, Phys. Rev. A **67**, 030702(R) (2003)
20. M.E. Galassi, R.D. Rivarola, P.D. Fainstein, Phys. Rev. A **70**, 032721 (2004)
21. M. Roy Chowdhury, L.C. Tribedi, J. Phys. B **50**, 155201 (2017)